presented in Table II. The data presented indicate that while the solid solutions are efficient, long-lived emissive hosts ($\phi_r \sim 0.2$; $\tau \sim 150\ \mu s$), they are somewhat less so than HUAs and HUP. In making this statement, we believe it is worth emphasizing that dehydration, which can reduce the PL intensity and lifetime of all these samples, may affect these comparisons. On the other hand, the HUPAs samples all seem to have similar properties, and we expect that the less uniform environment that emitting UO_2^{2+} moieties will see in the HUPAs samples might well promote nonradiative processes. As Table II indicates, k_r values are within a factor of 2 for all the samples examined, whereas k_{nr} decreases by factors of up to 3 and 10 in passing from the solid solutions to HUAs and HUP, respectively.

Conclusion

We have shown in this paper that HUP and HUAs are miscible, yielding the $HUO_2(PO_4)_{1-X}(AsO_4)_X$ (HUPAs) family of luminescent layered solids. With the rich intercalation chemistry that HUP and HUAs possess, the HUPAs solids represent an emissive host system with tunable lattice parameters than can be used to optically and structurally monitor intercalation reactions and host-guest interactions.

Acknowledgment. We are grateful to the Office of Naval Research for generous support of this work. We also thank Qunyin Xu for assistance with the TGA and DTA analyses and Drs. M. Markovič and L. F. Dahl for their helpful comments.

Registry No. $UO_2(NO_3)_2$, 10102-06-4; H_3PO_4, 7664-38-2; H_3AsO_4, 7778-39-4; $HUO_2(PO_4)_{0.22}(AsO_4)_{0.78}\cdot 4H_2O$, 113160-03-5; $HUO_2(PO_4)_{0.52}(AsO_4)_{0.48}\cdot 4H_2O$, 113160-05-7; $HUO_2(PO_4)_{0.81}(AsO_4)_{0.19}\cdot 4H_2O$, 113160-07-9.

Supplementary Material Available: Listings of $1/d^2$ values and *hkl* assignments (7 pages). Ordering information is given on any current masthead page.

(18) Wrighton, M. S.; Ginley, D. S. Morse, D. L. *J. Phys. Chem.* **1974**, *78*, 2229.

Contribution from the School of Chemical Sciences, University of Georgia, Athens, Georgia 30602, Departmento de Quimica, Universidad Nacional de Colombia, Bogota, Colombia, and Centro de Quimica Estrutural, Universidade Nova de Lisboa, 1000 Lisbon, Portugal

Electronic and Magnetic Properties of Nickel-Substituted Rubredoxin: A Variable-Temperature Magnetic Circular Dichroism Study

Andrzej T. Kowal,[1a] Isabel C. Zambrano,[1b] Isabel Moura,[1c] Jose J. G. Moura,[1c] Jean LeGall,[1a] and Michael K. Johnson*[1a]

Received August 26, 1987

Ni(II)-substituted rubredoxins from *Desulfovibrio gigas*, *Desulfovibrio vulgaris*, and *Clostridium pasteurianum* have been prepared and characterized by room-temperature UV-visible absorption and low-temperature MCD spectroscopy. The results are compared with those obtained for the crystallographically defined analogue complex $(Ph_4P)_2Ni(SPh)_4$. The Ni(II) sites in both the biological and inorganic compounds are found to be high spin, with very similar electronic and magnetic properties. The results are interpreted in terms of tetragonally distorted tetrahedral thiolate coordination for Ni(II), resulting in a $^3A_2$ ground state, under D_{2d} symmetry, that is subject to large axial zero-field splitting. Studies of the temperature dependence of the solution MCD spectra facilitate quantitative assessment of the axial zero-field splitting parameters; $D = 55\ cm^{-1}$ for Ni(II)-substituted Rd and $D = 44\ cm^{-1}$ for $Ni(SPh)_4^{2-}$. The properties of Ni(II) sites in hydrogenases are discussed in light of these results.

Introduction

Nickel has recently been shown to be present in at least four distinct types of biological systems:[2,3] urease from plant cells; hydrogenases from sulfate-reducing, methanogenic, photosynthetic, nitrogen-fixing, and "Knallgas" bacteria; CO dehydrogenase from acetogenic bacteria; a low molecular weight tetrapyrrole prosthetic group, factor F_{430}, which is present in methanogenic bacteria. In each instance the available spectroscopic data indicate that the nickel has a unique coordination environment. For hydrogenases EXAFS,[4-6] EPR,[7] and MCD[8] spectroscopies have provided evidence for sulfur coordination of a monomeric nickel center in the oxidized enzymes. However, there are presently few monomeric nickel thiolate complexes that could serve as model compounds and thereby facilitate detailed characterization of the ligand environment and coordination geometry.

In this work, we report spectroscopic investigations of nickel substituted rubredoxins, in which monomeric Ni(II) is ligated by four cysteinyl sulfur atoms. The electronic and magnetic properties of the Ni-substituted rubredoxins and the structurally well-characterized analogue complex $(Ph_4P)_2Ni(SPh)_4$[9,10] have been investigated by UV-visible adsorption and variable-temperature MCD spectroscopies. The results indicate tetragonally distorted tetrahedral nickel thiolate coordination and provide insight into the nature and magnitude of the splitting of the electronic ground state. The coordination of nickel in hydrogenases is discussed in the light of these results.

Experimental Section

Preparation of Compounds. Rubredoxin (Rd) was purified to homogeneity from *Desulfovibrio gigas*, *Desulfovibrio vulgaris*, and *Clostridium pasteurianum* by using the published procedures.[11] The experi-

(1) (a) University of Georgia. (b) Universidad Nacional de Colombia. (c) Universidade Nova de Lisboa.
(2) Thauer, R. K.; Diekert, G.; Schönheit, P. *Trends Biochem. Sci. (Pers. Ed.)* **1980**, *11*, 304.
(3) Thomson, A. J. *Nature (London)* **1982**, *298*, 602.
(4) Lindahl, P. A.; Kojima, R. P.; Hausinger, R. P.; Fox, J. A.; Teo, B. K.; Walsh, C. T.; Orme-Johnson, W. H. *J. Am. Chem. Soc.* **1984**, *106*, 3062.
(5) Scott, R. A.; Wallin, S. A.; Czechowski, M.; DerVartanian, D. V.; LeGall, J.; Peck, H. D., Jr.; Moura, I. *J. Am. Chem. Soc.* **1984**, *106*, 6864.
(6) Scott, R. A.; Czechowski, M.; DerVartanian, D. V.; LeGall, J.; Peck, H. D., Jr.; Moura, I. *Rev. Port. Quim.* **1985**, *27*, 67.
(7) Albracht, S. P. J.; Kröger, A.; Van der Zwaan, J. W.; Unden, G.; Böcher, R.; Mell, H.; Fontijn, R. D. *Biochim. Biophys. Acta* **1986**, *874*, 116.
(8) Johnson, M. K.; Zambrano, I. C.; Czechowski, M. H.; Peck, H. D., Jr.; DerVartanian, D. V.; LeGall, J. *Biochem. Biophys. Res. Commun.* **1985**, *128*, 220.
(9) Holah, D. G.; Coucouvanis, D. *J. Am. Chem. Soc.* **1975**, *97*, 6917.
(10) Swenson, D.; Baenziger, N. C.; Coucouvanis, D. *J. Am. Chem. Soc.* **1978**, *100*, 1932.
(11) (a) Moura, I.; Bruschi, M.; LeGall, J.; Moura, J. J. G.; Xavier, A. V. *Biochem. Biophys. Res. Commun.* **1977**, *75*, 1037. (b) Bruschi, M.; LeGall, J. *Biochim. Biophys. Acta* **1972**, *263*, 279. (c) Lovenberg, W. *Methods Enzymol.* **1971**, *24*, 477.

0020-1669/88/1327-1162$01.50/0

mental procedures used for the preparation of apo-Rds and the reconstitution of the active center with nickel are described in detail elsewhere.[12] The apo-protein was prepared by precipitation with trichloroacetic acid and reconstituted by adding a stoichiometric amount of nickel(II) chloride. The reconstituted protein was then purified by gel filtration. Metal analysis was performed by plasma emission spectroscopy on a Jarrell-Ash Model 750 AtomComp. Protein concentrations were determined by the Lowry method.[13] Samples used for low-temperature MCD investigations contained 50% (v/v) ethylene glycol to enable optical quality glasses to be formed on freezing. The presence of ethylene glycol had no effect on the room-temperature absorption spectrum of the samples.

$(Ph_4P)_2Ni(SPh)_4$ was prepared by the published method.[9] Solutions in dry acetonitrile or a 50/50 DMF/toluene mixture were stable only in the presence of a large excess of KSPh and were prepared and handled anaerobically under argon in a Vacuum Atmospheres drybox (<1 ppm O_2). A 50/50 DMF/toluene mixture was used as solvent for low-temperature MCD measurements since it forms a glass on freezing. Sample concentrations were based on $\epsilon_{680} = 327\ M^{-1}\ cm^{-1}$.[9]

Physical Measurements. UV–visible absorption measurements were made by using a Cary 219 spectrophotometer. MCD spectra were recorded by using an Oxford Instruments SM3, split-coil, superconducting magnet mated to a Jasco J500C spectropolarimeter. Spectra were recorded digitally with a Jasco DP-500N data processor interfaced to an IBM PC-XT microcomputer. Sample temperatures were measured by using calibrated carbon glass resistors (Lake Shore Cryogenics) placed both directly above and below the sample and controlled by a Rh/Fe resistor and heater connected to an Oxford Instruments DTC2 temperature controller. Magnetic field calibration was carried out with a transverse Hall probe (Lake Shore Cryogenics). MCD spectra are corrected for natural CD and expressed as the difference in the molar extinction coefficients for left and right circularly polarized light, $\Delta\epsilon = \epsilon_L - \epsilon_R$. Magnetic fields, path lengths, and sample concentrations are given in the figure legends.

Results

Ni-Substituted Rubredoxins. Samples of Ni-substituted Rd were prepared from apoproteins isolated from *D. gigas*, *D. vulgaris*, and *C. pasteurianum*. On the basis of the Ni and protein analyses, each contained 0.95 ± 0.2 Ni/molecule. The native Fe Rds from these bacteria are very similar, i.e. molecular masses around 6000 Da, four highly conserved cysteine residues, and identical EPR, MCD, and Mössbauer characteristics. Likewise, the Ni-substituted Rds were identical as judged by the UV–visible absorption and MCD spectra. One problem encountered in preparing samples suitable for MCD spectroscopy, was the difficulty in removing all the Fe from the apoprotein prior to reconstitution with Ni. The apoprotein has an extremely high affinity for Fe and the native Fe Rd exhibits intense MCD transitions at low temperatures throughout the UV–visible region. Samples completely free of Fe Rd were obtained for Ni-substituted *D. gigas* Rd by repeated precipitation of the apoprotein with trichloroacetic acid. The results shown below are exclusively for these samples of Ni-substituted *D. gigas* Rd. However, identical spectra, except for minor contributions from Fe Rd that are only apparent in the MCD data, were obtained for the Ni-substituted Rds from *C. pasteurianum* and *D. vulgaris*.

Figure 1 shows the room-temperature absorption spectrum and MCD spectra recorded at temperatures between 4.2 and 137 K with a magnetic field of 4.5 T of Ni-substituted *D. gigas* Rd in the wavelength region 300–800 nm. The room-temperature absorption is composed of two intense bands at 360 and 450 nm ($\epsilon_{360} = 5460\ M^{-1}\ cm^{-1}$, $\epsilon_{450} = 3200\ M^{-1}\ cm^{-1}$), which are attributed to S → Ni(II) charge-transfer transitions, and two weaker bands at 670 and 720 nm ($\epsilon_{670} = 385\ M^{-1}\ cm^{-1}$, ϵ_{720} and $460\ M^{-1}\ cm^{-1}$), which arise from Ni(II) d–d transitions. On the basis of published spectra of structurally well-characterized Ni(II) complexes with thiolate ligands[9,10,14–16] and the results discussed below for Ni-

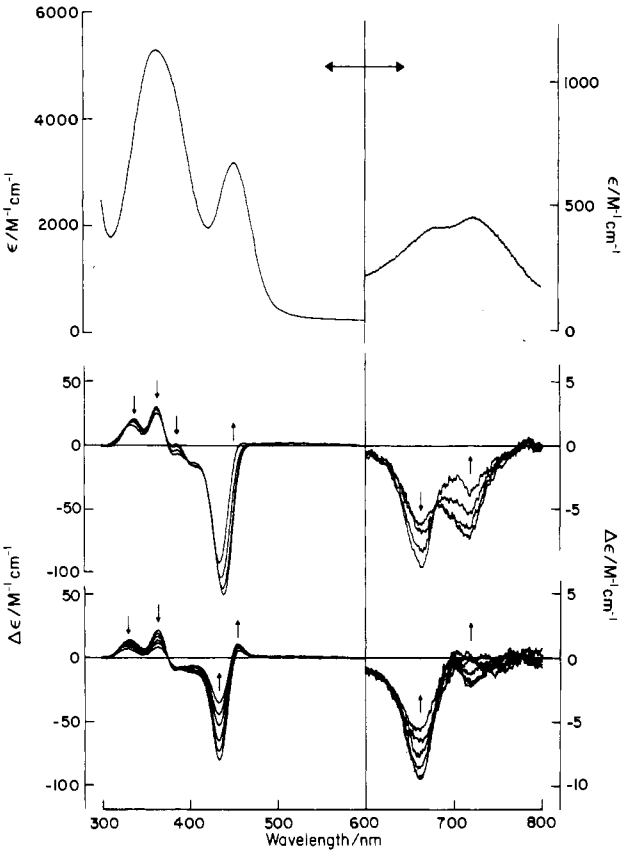

Figure 1. Room-temperature absorption and low-temperature MCD spectra of Ni-substituted *D. gigas* rubredoxin. The sample concentration was 1 mM in 0.1 M Tris/HCl buffer, pH 7.4, with 50% (v/v) ethylene glycol. Upper panel: room temperature absorption. Middle panel: MCD spectra at 4.2, 19.0, 28.4, and 40.2 K; magnetic field, 4.5 T; path length, 0.167 cm. Lower panel: MCD spectra at 53.1, 61.3, 71.6, 89.8, 108.1, and 137.0 K; magnetic field, 4.5 T; path length, 0.167 cm. Vertical arrows indicate the direction of change in MCD intensity at discrete wavelengths with increasing temperature.

$(SPh)_4^{2-}$, the bands at 670 and 720 nm are assigned to components of the $^3T_1(F)$ to $^3T_1(P)$ d–d transition of Ni(II) in an approximately tetrahedral coordination geometry.

The corresponding MCD spectra exhibit bands in analogous regions that display unusual temperature dependence. Below 15 K, the MCD spectrum is independent of temperature and all bands are found to be linearly dependent on the magnetic field strength. Such behavior is indicative of a nondegenerate state as the lowest energy component of the ground state multiplet. The transitions are assigned to *B* terms[17] originating from field-induced mixing of the levels of the ground state manifold. For the observed line widths, *A* terms would be expected to be of negligible importance at low temperatures. Pronounced changes in the MCD spectrum occur at temperatures above 15 K. The negative bands at 437 and 718 nm and the positive bands at 338 and 363 nm decrease with increasing temperature, concomitant with the appearance of a positive band at 454 nm. With increasing temperature, the negative band at 664 nm shows an initial increase and subsequent decrease in intensity with the maximum occurring around 50 K. This complex temperature dependence is best interpreted in terms of population of a degenerate low-lying state that gives rise to *C* terms exhibiting inverse temperature dependence.

The energy separation, ΔE, between the nondegenerate and degenerate components (labeled 1 and 2, respectively) of the ground-state multiplet can be assessed by plotting the MCD

(12) Moura, I.; Teixeira, M.; Saint-Martin, P.; Xavier, A. V.; LeGall, J.; Moura, J. J. G., manuscript in preparation.
(13) Lowry, O. H.; Rosebrough, N. J.; Fan, A. L.; Randall, R. J. *J. Biol. Chem.* **1951**, *193*, 265.
(14) Churchill, M. R.; Cooke, J.; Fennessey, J. P.; Wormald, J. *Inorg. Chem.* **1971**, *10*, 1031.
(15) Davison, A.; Switkes, E. S. *Inorg. Chem.* **1971**, *10*, 837.
(16) Rosenfield, S. G.; Armstrong, W. H.; Mascharak, P. K. *Inorg. Chem.* **1986**, *25*, 3014.
(17) We use the customary nomenclature for MCD parameters; see, for example: Buckingham, A. D.; Stephens, P. J. *Annu. Rev. Phys. Chem.* **1966**, *17*, 399.

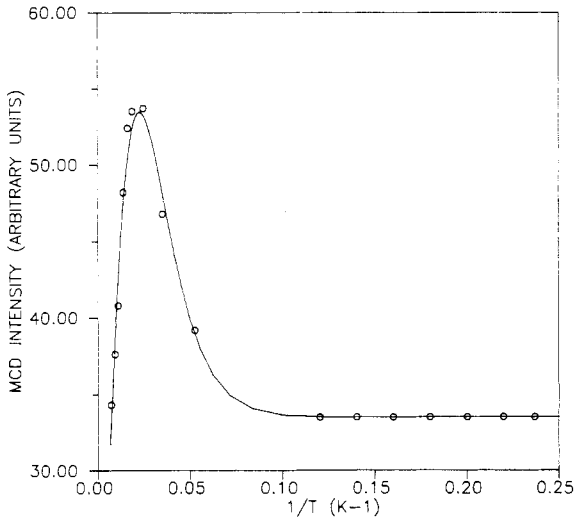

Figure 2. Temperature dependence of the MCD intensity of Ni-substituted *D. gigas* rubredoxin at 664 nm. Solid line is best fit to eq 1: $d_2 = 2$, $\Delta E = 55.5$ cm^{-1}, and $C_2 = 3381$ (arbitrary units).

intensity, ΔA, at a discrete wavelength as a function of inverse temperature and fitting to eq 1, where α_1 and α_2 are the fractional

$$\Delta A = \alpha_1 B_1 + \alpha_2 C_2/kT, \quad (1)$$

$$\alpha_1 = 1/[1 + d_2 \exp(-\Delta E/kT)]$$

$$\alpha_2 = d_2 \exp(-\Delta E/kT)/[1 + d_2 \exp(-\Delta E/kT)]$$

populations of components 1 and 2, respectively, d_2 is the degeneracy of component 2, B_1 is the magnitude of the B term from component 1 at temperatures such that only the nondegenerate state is populated, and C_2 is the magnitude of the C term from component 2. The validity of such a treatment rests on three assumptions. First, Curie law behavior is assumed for the transitions from component 2. This is reasonable since this level only becomes significantly populated at temperatures above 20 K, and saturation effects are not expected to be significant at this temperature for a magnetic field of 4.5 T. Second, it assumes that no additional components of the ground-state manifold are significantly populated over the temperature range of the experiment, 4.2 to 137 K. Third, the B term from component 1 is assumed to be temperature independent over the entire temperature range. B terms that originate from mixing of closely spaced levels of a ground-state manifold can be temperature dependent in the event that the mixing state becomes thermally populated.[18] The second and third assumptions are valid if the ground-state has a large tetragonal distortion. As discussed below, there is good reason to believe that this is indeed the case.

Figure 2 shows the temperature dependence of the MCD intensity for the transition at 664 nm. This wavelength was chosen because of the greater accuracy in fitting data that displays an initial increase and subsequent decrease as a function of increasing temperature. The data afforded satisfactory fits to eq 1 (i.e. within the estimated experimental error of the data points) using $d_2 = 2$ or 3. The best fit data for $d_2 = 2$ is shown in Figure 2. Nonlinear least-squares fitting gave values of $\Delta E = 55.5$ and 62.2 cm^{-1} for a doubly and triply degenerate upper level, respectively. From these values the form of the MCD spectra originating from both the nondegenerate and degenerate levels were deduced at a temperature where the upper level affords the optimal contribution to the MCD intensity, i.e. 61.3 K. This procedure entailed calculating the fractional population of the nondegenerate ground state at the prescribed temperature and subtracting a proportional amount of the 4.2 K spectrum from the spectrum at 61.3 K. Analogous results were obtained irrespective of whether a doubly or triply degenerate excited state was assumed, and the spectra

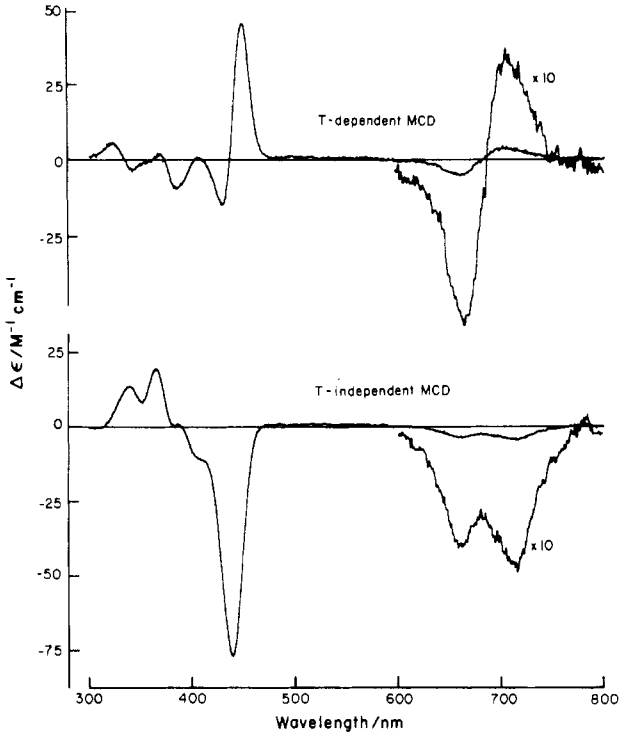

Figure 3. Temperature-dependent and temperature-independent components of the MCD spectra of Ni-substituted *D. gigas* rubredoxin. Sample as described in Figure 1. Conditions: temperature, 61.3 K; magnetic field, 4.5 T. Upper spectrum: temperature-dependent MCD from low-lying degenerate excited state. Lower spectrum: temperature-independent MCD from nondegenerate ground state.

are shown in Figure 3. Clearly the transitions from both levels occur at approximately the same energies, showing that both levels are components of a common spin system. Therefore, we discount the possibility that the unusual temperature dependence of the MCD spectra arises from closely spaced states with a total spin of $S = 0$ and 1, respectively. Such a situation could conceivably occur for coordination geometries intermediate between tetrahedral ($S = 1$, ground state) and square planar ($S = 0$, ground state).

$(Ph_4P)_2Ni(SPh)_4$. Room-temperature absorption and MCD spectra recorded at temperatures between 4.2 and 88.7 K with a magnetic field of 4.5 T for $(Ph_4P)_2Ni(SPh)_4$ in a 50/50 DMF/toluene mixture with excess KSPh, are shown in Figure 4. Very similar absorption spectra were obtained in acetonitrile in the presence of excess KSPh, except that the band at 740 nm is slightly less pronounced, appearing as a shoulder centered at 725 nm on the band at 676 nm. The spectrum in acetonitrile is in excellent agreement with previously published data.[9] The solution absorption spectra for $Ni(SPh)_4^{2-}$ closely resemble those obtained for Ni-substituted Rds, particularly in the d–d region. While two S → Ni(II) charge-transfer bands are also observed, they occur to lower energy, 460 and 510 nm, than the equivalent bands in Ni-substituted Rds. The similarities in the absorption spectra suggest similar coordination environments for Ni(II) in $Ni(SPh)_4^{2-}$ and Ni-substituted Rd.

The close similarity in the electronic properties of $Ni(SPh)_4^{2-}$ and Ni-substituted rubredoxins in solution is even more apparent in the low-temperature MCD data. Except for the difference in the energies of the charge-transfer bands, the overall form of the MCD spectra as well as the unusual temperature dependence are similar for both $Ni(SPh)_4^{2-}$ and Ni-substituted Rd. For $Ni(SPh)_4^{2-}$ the MCD spectrum is invariant as a function of temperature below 10 K, and the changes that occur with increasing temperature above 10 K directly parallel those described above for Ni-substituted Rd and may be explained in an analogous manner. As for Ni-substituted Rd, the energy separation between the nondegenerate and degenerate components of the ground-state multiplet were assessed by fitting a plot of MCD intensity at 664 nm versus inverse temperature to eq 1; see Figure 5. Satisfactory

(18) Collingwood, J. C.; Day, P.; Denning, R. G. *J. Chem. Soc., Faraday Trans. 1* **1973**, *269*, 591.

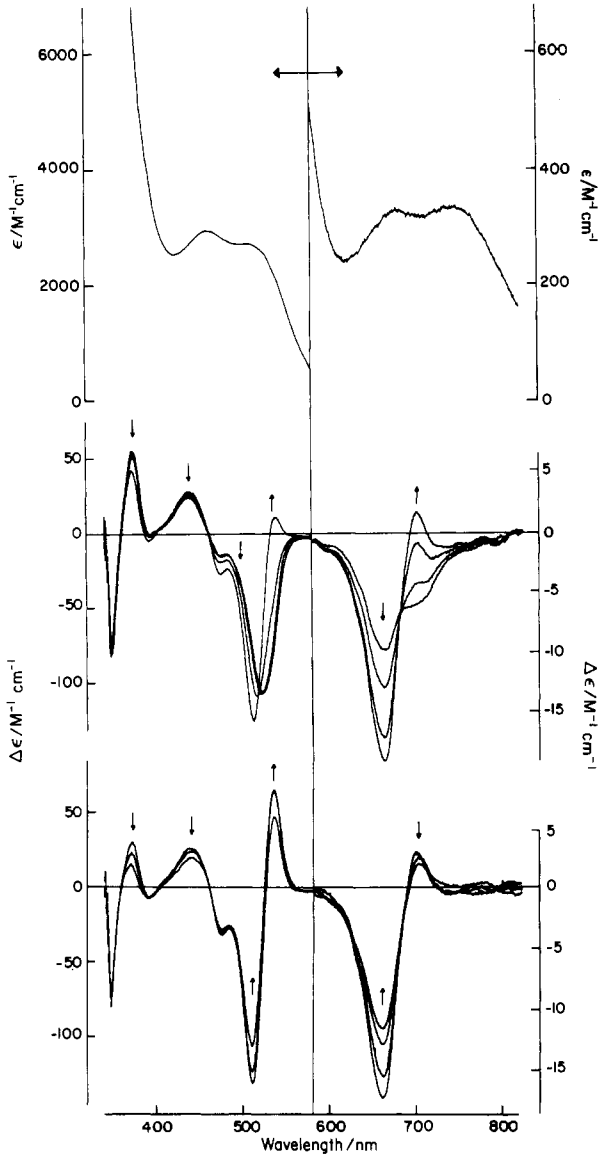

Figure 4. Room-temperature absorption and low-temperature MCD spectra of $(Ph_4P)_2Ni(SPh)_4$. Conditions: sample concentration, 0.55 mM (300–580 nm) and 1.52 mM (580–800 nm); solvent 50/50 DMF/toluene mixture with 10-fold stoichiometric excess of KSPh. Upper panel: Room-temperature absorption. Middle panel: MCD spectra at 4.2, 8.2, 18.5, and 27.5 K; magnetic field, 4.5 T, path length, 0.174 cm (300–580 nm); MCD spectra at 4.2, 18.7, 27.8, and 38.7 K; magnetic field, 4.5 T, path length, 0.172 cm (580–800 nm). Lower panel: MCD spectra at 37.3, 47.1, and 60.6 K; magnetic field, 4.5 T, pathlength, 0.174 cm (300–580 nm); MCD spectra at 50.2, 60.6, 76.4, and 88.7 K; magnetic field, 4.5 T; path length, 0.172 cm (580–800 nm). Vertical arrows indicate the direction of change in MCD intensity at discrete wavelengths with increasing temperature.

fits were obtained for a doubly degenerate level at 44.3 cm^{-1} or a triply degenerate level at 50.0 cm^{-1}, above the singlet state. These energy separations are lower than those found for the Ni(II)-substituted Rds by approximately 10 cm^{-1}. The energy separations were used to obtain the form of the MCD transitions from each component of the ground-state multiplet at 60.4 K (see Figure 6) so as to enable direct comparison with the equivalent spectra for Ni(II)-substituted Rds, (see Figure 3). Apart from the difference in the intensities of the MCD signals from the upper degenerate levels and the enhanced intensity for the higher energy d–d band originating from the nondegenerate component of ground state of $Ni(SPh)_4^{2-}$, the spectra display marked similarities.

Discussion

The close correspondences in both the UV–visible absorption and low-temperature MCD characteristics of Ni-substituted Rds

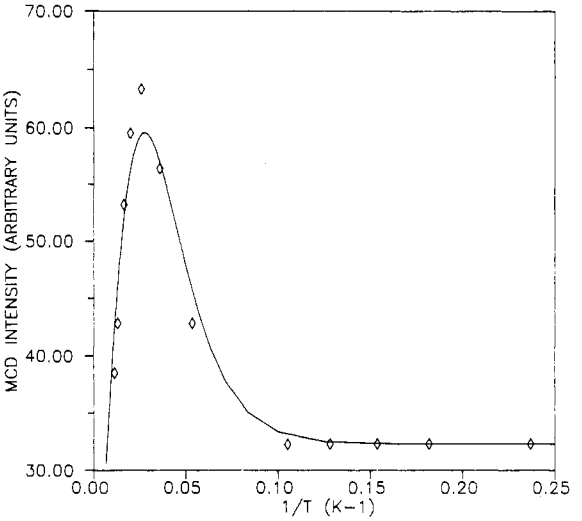

Figure 5. Temperature dependence of the MCD intensity of $(Ph_4P)_2Ni(SPh)_4$ at 664 nm. Solid line is best fit to eq 1: $d_2 = 2$, $\Delta E = 44.3$ cm^{-1}, and $C_2 = 3403$ (arbitrary units).

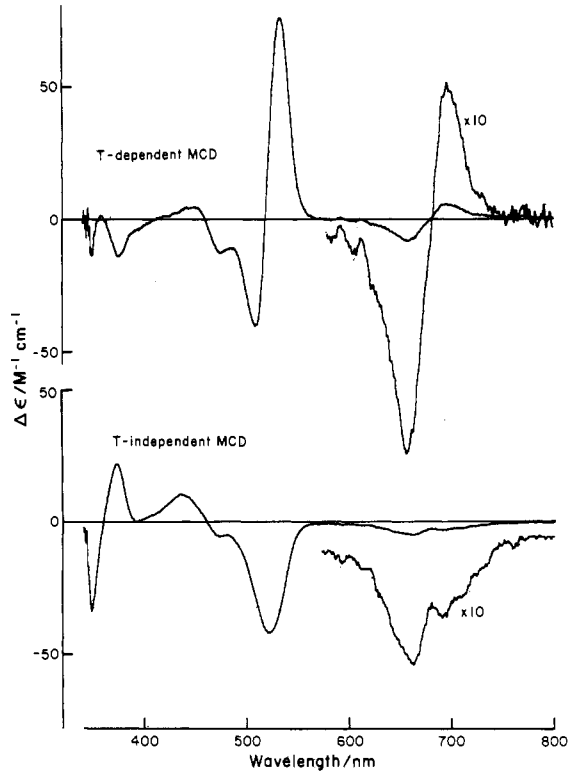

Figure 6. Temperature-dependent and temperature-independent components of the MCD spectra of $(Ph_4P)_2Ni(SPh)_4$. Sample as described in Figure 4. Conditions: temperature, 60.6 K; magnetic field, 4.5 T. Upper spectrum: temperature-dependent MCD from low-lying degenerate excited state. Lower spectrum: temperature-independent MCD from nondegenerate ground state.

and $Ni(SPh)_4^{2-}$ indicate very similar coordination environments for the metal centers. The only other published biological example of a monomeric Ni(II) center ligated by four crysteine residues is that of Ni(II)-substituted aspartate transcarbamoylase.[19] Comparison of the UV–visible absorption spectra of Ni(II)-substituted Rds and aspartate transcarbamoylase points to identical Ni(II) coordination in both proteins. As discussed below the results presented here are consistent with a tetragonally distorted tetrahedral NiS_4 center in both the biological and inorganic complexes.

(19) Johnson, R. S.; Schachman, H. K. *Proc. Natl. Acad. Sci. U.S.A.* **1980**, *77*, 1995.

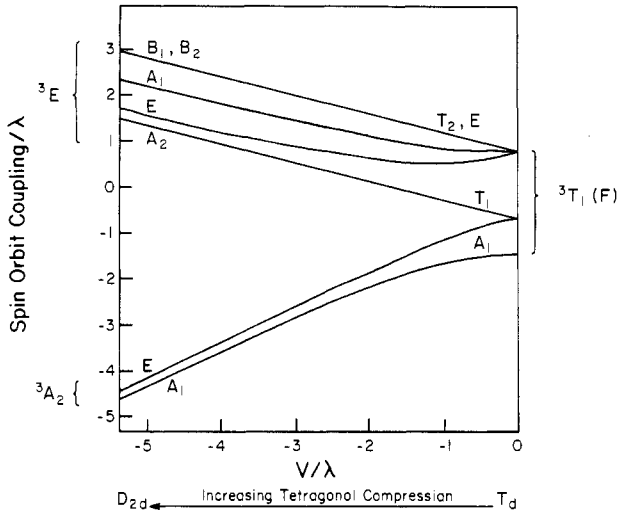

Figure 7. Effect of spin–orbit coupling and tetragonal distortion on the $^3T_1$ ground state (modified from ref 18).

Evidence for a tetrahedral or distorted tetrahedral coordination geometry for Ni(II) in solutions of $Ni(SPh)_4^{2-}$ and Ni-substituted Rds comes from both the spectroscopic and magnetic properties. The variable-temperature MCD data can only be interpreted in terms of a high-spin, $S = 1$, ground state and the magnitude and location of the d–d transitions are indicative of approximately tetrahedral thiolate coordination. The variability in the absorption spectra of $Ni(SPh)_4^{2-}$ as a function of the solvent may reflect a tetrahedral ($S = 1$) $\rightleftharpoons$ planar ($S = 0$) equilibrium in solution. The existence of such an equilibrium is also suggested by measurements of the magnetic susceptibility in solution,[9,16] which found the magnetic moment to be dependent on concentration, solvent, and time. On the basis of low solution magnetic moments, a similar equilibrium was proposed for the (bis(thiophosphino)-amido)nickel complexes.[15] However, even if such an equilibrium exists for $Ni(SPh)_4^{2-}$ in solution, it does not affect the analysis of the MCD data for the $S = 1$ component, since the diamagnetic, $S = 0$ component would be expected to exhibit very weak, temperature-independent MCD bands.

Analysis of the temperature dependence of the MCD spectra of Ni(II)-substituted Rds and $Ni(SPh)_4^{2-}$ reveals that the ground-state manifold originating from the parent $^3T_1(F)$ state under tetrahedral symmetry, has a nondegenerate level as the lowest energy component with a doubly or triply degenerate component approximately 50 cm^{-1} higher in energy. The energy levels resulting from the first-order treatment of a tetragonal compression and spin-orbit coupling with a $^3T_1$ state are depicted in Figure 7 as a function of the relative tetragonal distortion, V/λ, where λ is the spin–orbit coupling constant. Inspection of Figure 7 shows that both T_d and D_{2d} geometries are consistent with the MCD analysis. For the T_d case the separation between the A_1 and T_1 spin-orbit components of the $^3T_1$ ground state would equate to $3/4\lambda$, whereas for the D_{2d} case the separation between the E and A_1 components of the $^3A_2$ ground state would equate to D, the axial zero-field splitting parameter, under the spin Hamiltonian formalism.

While it is difficult to decide between these alternatives on the basis of the MCD data alone, the X-ray crystallographic data for $(Ph_4P)_2Ni(SPh)_4$ does show a highly distorted tetrahedral NiS_4 core that approaches D_{2d} symmetry.[10] The suggestion that the tetragonal distortion that is observed in the X-ray structure of $(Ph_4P)_2Ni(SPh)_4$ is a consequence of crystal packing effects[10] is unlikely for two reasons. First, the distortion for $(Ph_4P)_2M(SPh)_4$, where M = Cd(II), Zn(II), Co(II), Mn(II), and Ni(II), is much more pronounced for the Ni(II) complex of this isomorphous series.[10] Second, the distortion for the Ni(II) complex persists even with changes of counterion and thiolate.[16] Therefore, we interpret our spectroscopic and magnetic data for Ni(II)-substituted Rds and $Ni(SPh)_4^{2-}$ in solution in terms of a $^3A_2$ ground state under D_{2d} symmetry. Likewise the splitting of the Ni(II) d–d band in the 600–750-nm region that is apparent in both the absorption and MCD spectra can be attributed to a tetragonal distortion in the parent $^3T_1$ excited state.

The MCD measurements show that the $^3A_2$ ground states of both Ni(II)-substituted Rds and $Ni(SPh)_4^{2-}$ are subject to a large zero-field splittings ($D = 55$ and 44 cm^{-1}, respectively). As indicated in Figure 7, the zero-field splitting in the $^3A_2$ ground state is a consequence of mixing of the ^3E and $^3A_2$ components of the parent $^3T_1$ state via spin–orbit coupling. The close proximity of the ^3E excited state is, therefore, responsible for the unusually large zero-field splitting. Also, for such a ground state, the intensity of the MCD transitions originating from the degenerate upper level should be very dependent on the magnitude of any rhombic zero-field distortion. Such a distortion removes the degeneracy of the non-Kramers doublet, thereby quenching its angular momentum and eliminating MCD intensity. Therefore, the observed differences in the intensity of the MCD spectra originating from the doubly degenerate upper level, cf. Figures 3 and 6, can readily be rationalized in terms of larger rhombic zero-field distortion in the case of Ni(II)-substituted Rd.

In general, tetracoordinated nickel complexes with chelates possessing sulfhydryl groups are found to have square-planar coordination geometries.[14,15] We attributed the distorted tetrahedral coordination for Ni(II) in Rds and aspartate transcarbamoylase to constraints on the orientation of the cysteine residues that are imposed by the folding of the polypeptides. In the case of $Ni(SPh)_4^{2-}$, steric factors involving the bulky Ph groups are probably responsible for the observed coordination geometry.

Finally, we turn our attention to the implications of these results with regard to the coordination of Ni(II) centers in hydrogenases. We have investigated the low-temperature MCD spectra of the Ni-containing hydrogenases from *D. gigas* and *Methanobacterium thermoautotrophicum*, both as isolated forms and at various stages of reduction by both hydrogen and dithionite.[20] While electronic transitions (S $\rightarrow$ Ni(III) charge transfer and Ni(III) d–d) from the $S = {}^1/_2$ Ni(III) center in as isolated samples have been identified, no MCD bands that could be attributed to high-spin, paramagnetic Ni(II) species have been observed during redox titrations. Therefore, we conclude that nickel(II) thiolate centers in hydrogenases are probably low spin ($S = 0$), which suggests square-planar, square-pyramidal, or axially distorted octahedral coordination geometry.

Acknowledgment. This research was supported by grants from the National Science Foundation DMB 8796212 (to M.K.J.), Junta National de Investigacao Cientifica and Tecnologica (to J.J.G.M.), and CEC BAP-0259-P-(TT) (to J.J.G.M.). M.K.J. is the recipient of an Alfred P. Sloan Foundation fellowship.

Registry No. $(Ph_4P)_2Ni(SPh)_4$, 57927-74-9.

(20) Johnson, M. K.; Zambrano, I. C.; Czechowski, M. H.; Peck, H. D., Jr.; DerVartanian, D. V.; LeGall, J. In *Frontiers of Bioinorganic Chemistry*; Xavier, A. V., Ed.; VCH Publishers: Deerfield Beach, FL, 1986; p 36 and unpublished results.